Proceedings World Geothermal Congress 2015
Melbourne, Australia, 19-25 April 2015

A Geothermal Exploration MT Data Set and its 3-D Inversion Using Two Different Codes: An Example from Western Turkey

Wouter A. van Leeuwen[1,2], Kris Marnette[3], Ruud J. Schotting[1] and Mark Muller[4]

[1]Utrecht University, Faculty of Geosciences, Budapestlaan 4, 3584 CD Utrecht, the Netherlands

[2]IF Technology, Velperweg 37, 6824BE Arnhem, the Netherlands

[3]Transmark Renewables Products B.V., Herengracht 386, 1016 CJ Amsterdam, the Netherlands

[4]Independent Consultant, 31 Williams Place South, Dublin, Ireland

E-mail: w.a.vanleeuwen@uu.nl

Keywords: Magnetotellurics, processing, 3-D inversion, geothermal exploration

ABSTRACT

In June 2013 a 51-station magnetotelluric (MT) survey was carried out to investigate the geothermal prospectivity of an area located in the Aegean Coastal Belt in northwestern Turkey. The metamorphic unit that is generally inferred to host the geothermal reservoir is of Paleozoic age and contains a granitic batholith which intruded the unit during volcanic activity in the Oligo-Miocene period. These metamorphic rocks are furthermore overlain by a Miocene volcanogenic unit which developed during several phases of volcanism. The youngest geological unit consists of alluvial sediments deposited during the Quarternary. Structurally, the area was formed by extensional tectonic movements associated with N-NE to S-SW oriented fault systems and normal faulting.

The acquired MT time-series data are processed using industry standard processing software. After data processing, Egbert's (2012) ModEM code and Mackie's (2012) magnetotelluric inversion code are used for the 3-D inversion of the MT responses. The 3-D modelling results are compared and we evaluate the differences between the two 3-D resistivity models and discuss the implications any differences and similarities have for the definition of the geothermal reservoir and resource.

1. INTRODUCTION

Geothermal energy resources in Turkey are related to the tectonic processes and structures associated with the geological development of the Menderes Metamorphic Massif (MMM) which is bounded by the İzmir-Ankara mountain range at its western and northwestern boundaries. Recent north-south extensional tectonics, related to the northward movement of the Afro-Arabian Plate and the westward movement of the Anatolian Sub-plate, created several major east-west oriented grabens in southeastern Anatolia. The faults bounding these structures are open as a result of the extensional stress regime and allow for the deep circulation and heating of meteoric waters. The Northern Anatolian Fault Zone along the northern boundary of the Anatolian Sub-plate provides deep permeable flow channels for geothermal waters. This tectonics regime is associated with the high heat flow and associated geothermal systems throughout western Anatolia and along the Aegean Coastal Belt (Şerpen et al., 2009) as shown in Figure 1.

The development of the geothermal field investigated here is also associated with Miocene volcanism. The geothermal waters circulate in deep faults of the fracture systems associated with this volcanism (Şerpen et al., 2009).

The geothermal field discussed in this paper is situated at an undisclosed location in northwestern Turkey. It is one of several similar, low-to-medium temperature, geothermal fields, generally grouped within the Aegean Coastal Belt as shown in Figure 1. Geothermal systems formed along the edges of the tectonic grabens in this belt.

The geothermal energy potential in this area has been extensively studied previously (Şerpen et al., 2009) and a number of geothermal projects have recently been developed or are currently being developed. Numerous exploration licenses have been granted in the region. The exploration resistivity survey that forms the focus of this paper was conducted in June 2013 by a third party within the boundaries of one of these license areas with the aim of identifying the geothermal reservoir at depth. During the resistivity survey, 51 combined audiomagnetotellurics (AMT) and magnetotelluric (MT) soundings were measured, each for about 16 hours duration, with a remote-reference station operating simultaneously at a quiet location approximately 10 kilometers away.

As a first step the acquired (A)MT data were inverted in 1-D to create an initial 1-D model of the reservoir. Following that, 3-D inversion models were derived using two different codes - one of them being ModEM (Egbert & Kelbert, 2012) and the other being the proprietary CGG 3-D inversion code developed by Mackie (2012). The differences and similarities between the model results of these two 3-D inversion codes are discussed below.

Finally, since the 3-D modelling work presented is the work of third parties, we will propose some future processing and modelling strategies which are thought to improve the results considerably.

2. DATA ACQUISITION

A 51 (A)MT station resistivity survey was carried out in June and July 2013. During the MT recordings, an MT 'remote' station was operating simultaneously at a distance of approximately 10 km from the survey area. For the AMT data recordings no remote station was used. Consequently, the AMT data were processed using the local magnetic field only. The resistivity data was collected during two periods; one from 7 to 14 June 2013 and one from 27 June to 10 July 2013.

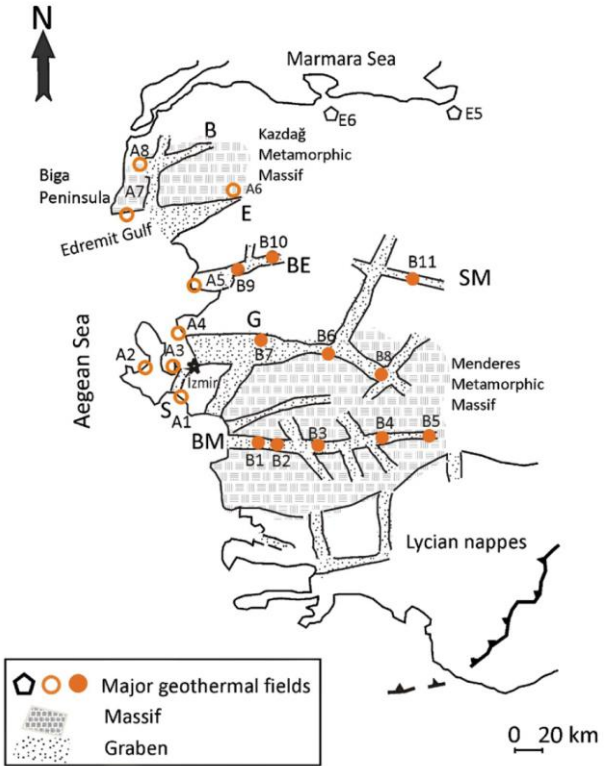

Figure 1. Geothermal fields in the Aegean Coastal Belt of western Anatolia and schematic overview of the geology of the region illustrating the main structural grabens: B = Bayramiç, E = Edremit, BE = Bergama, SM = Simav, G = Gediz, S= Seferihishar and BM = Büyük Menderes. Indicated with either A or B and a number are the known major geothermal fields in this area (Şerpen et al., 2009).

Both Phoenix MTU5's and Metronix ADU-07 instruments were used as data loggers during the resistivity survey. The stations measured with the Metronix instruments were all located in the eastern part of the survey area and were acquired during the 1st part of the survey, while the Phoenix instruments recorded data at stations located in the western part of the area during the 2nd part of the survey. The survey layout is illustrated in Figure 2. Stations using Phoenix instruments were recorded using both AMT (AMTC-30) and MT (MTC-50H) coils, with an AMT coil deployed as H_z for all measurements. At stations measuring with Metronix instruments, only one type of magnetic coil was deployed (MFS-06e coils). Data were acquired in a frequency range from 0.001 Hz to either 320 Hz - using the Metronix instruments - or 10,000 Hz - using the Phoenix instruments. In all instances, MT data were collected for 16 hours per station.

The stations were placed in an irregular grid with a station spacing varying from about 250 to 1,200 meters (see Figure 2).

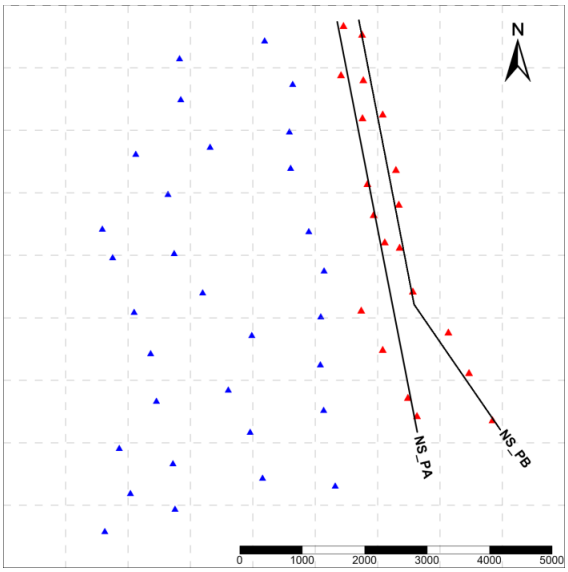

Figure 2: Station layout of the 51-station resistivity survey. Red stations were measured using Metronix instrumentation and blue stations using Phoenix instrumentation. Also plotted are the two north-south oriented profiles NS_PA and NS_PB. Scale bar shows meters.

3. DATA PROCESSING AND EVALUATION

Since the resistivity data were recorded by a third party, the time series processing is reviewed briefly below, after which the resulting resistivity data are evaluated.

3.1 Time series processing

All the resistivity data acquired were processed using existing "standard" software. This implies that the raw time series data recorded using Metronix instruments were processed to the transfer functions using the EMTF code developed by Egbert (1986), while the raw time series data acquired with Phoenix instruments were processed to the transfer functions using proprietary Phoenix software (SSMT2000 and MT Editor). As two different processing software codes were used, it is difficult to make an objective assessment of the data quality of the recorded time series data independently of the processing code used. EMTF uses a robust processing scheme, while the Phoenix software is developed around cascade decimation (Jones, 1989), but also applies a robust processing algorithm.

3.2 Data evaluation and preparation

Despite the differences in survey date, and hardware and software used for the two parts of the survey, the apparent resistivity and phase responses are predominantly consistent for all the measured stations. This consistency is illustrated in Figure 3 where the station P001 measured with Phoenix instrumentation and the station M001 measured with Metronix instrumentation are compared with each other.

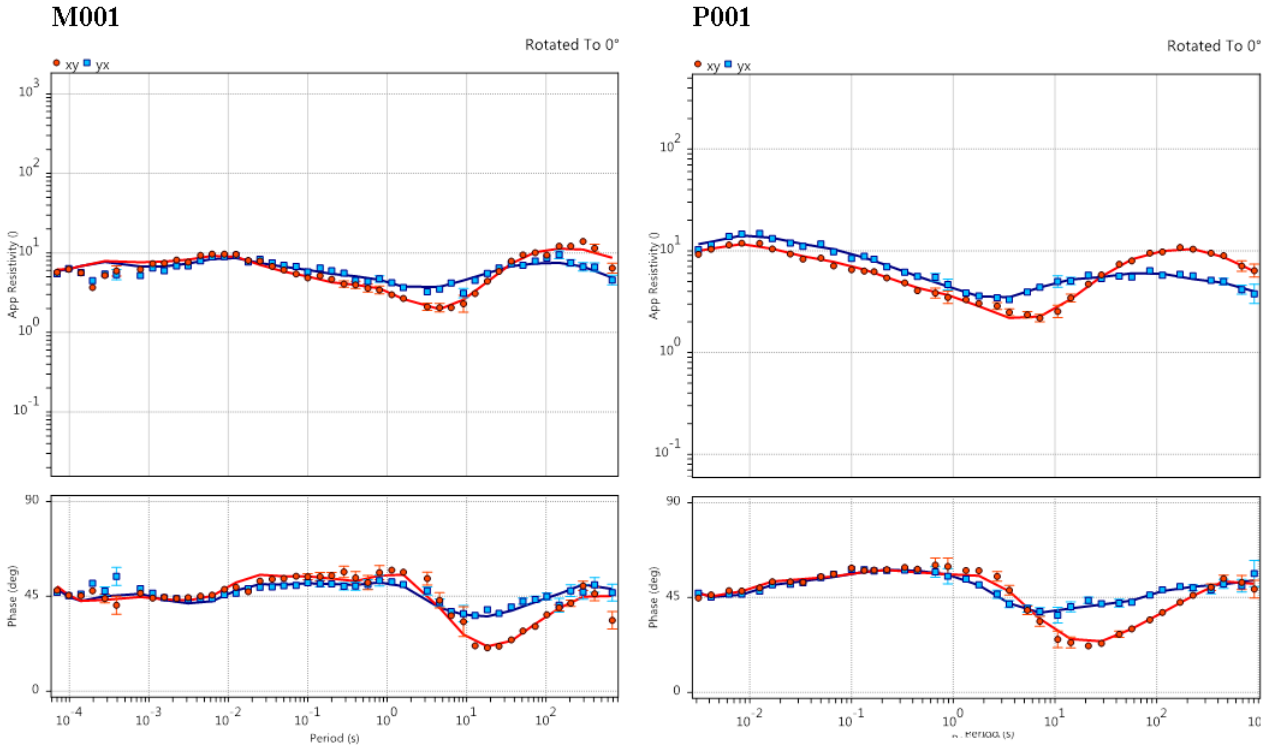

Figure 3: Station apparent resistivity and phase responses of Z_{xy} (red dots) and Z_{yx} (blue squares) for a station measured with Metronix equipment (left, M001) and a station measured with Phoenix equipment (right, P001). Subsequent D+ curves (solid lines) are plotted as well for both stations. These two sites are located about 2,000 m apart from each other.

A Rho+ (Parker & Whaler, 1981) or the more commonly used D+ (Parker & Booker, 1996) test is an effective means of testing the consistency between apparent resistivity and phase of the magnetotelluric data (except for the case of 3-D data, where the tests are not appropriate). Applying the D+ algorithm to the MT data showed (see Figure 3) that the phases and resistivities are in general consistent with each other.

There is, however, an inconsistency in the magnetic data between the two - Metronix and Phoenix - data sets when looking at the vertical magnetic transfer functions (tippers). The data measured with Metronix instruments and coils show consistent, clean tipper responses as illustrated in Figure 3 at station M001. In contrast, the vertical magnetic transfer function derived from the Phoenix instrument measurements is questionable at frequencies below 1 Hz, as illustrated at station P001, also plotted in Figure 3. The shape of the tipper data at station M001, characterised by larger amplitudes at longer periods, is also consistent with the presence of the conductive Mediterranean Sea present at the southern side of the survey area. The characteristics of the Phoenix tipper data are very noisy between 8 and 0.5 Hz (and therefore masked in Figure 4), with a near-zero response below 0.01Hz. This may be the result of recording the H_z component with an AMT (AMTC-30) coil rather than with an MT (MTC-50H) coil, as used for the horizontal components. Reprocessing of the tipper data, could be a double-check if the different frequency responses of the different coils are accounted for and will assess whether the Phoenix tipper characteristics resulted from the rapid drop-off in the amplitude response of the AMTC-30 coils at frequencies below 1 Hz.

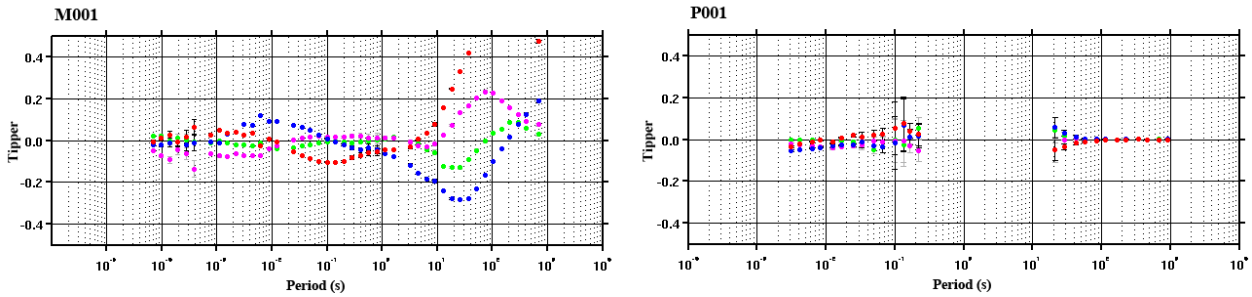

Figure 4: Vertical magnetic transfer function (tipper) of stations M001 (a Metronix instrument site) and P001 (a Phoenix instrument site). T_{zx}: magenta (real) and green (imaginary); T_{zy}: red (real) and blue (imaginary).

Static shift effects in the apparent resistivities can be recognized at some of the measured stations. No static shift correction was made before inverting the data.

Before running any inversion of MT data, spurious data points are often masked or smoothed to avoid unrealistic results in the resistivity models. Whereas for the 3-D inversion modelling using ModEM the input data after processing were left untouched, spurious data points were masked by the users of Mackie's code before inverting the station responses.

4. 1-D AND 3-D INVERSION MODELLING

As indicated before, two different codes were used to derive a 3-D inversion model of the exploration area. Both codes use a finite difference approach, while the differences between the two codes can be found in the solvers applied to the system of linear equations, the model grid and the boundary conditions applied. A detailed description of the similarities and differences between Egbert's and Mackie's approach is outside the scope of this paper. From now on, the 3-D inversion modelling carried out using Mackie's approach will be called "Code I', while the 3-D inversion modelling using Egbert's approach, or ModEM, will be called "Code II".

Similarly to the data processing, different strategies were used when inverting the MT data in 3-D using the two different codes, which makes it harder to interpret the differences between the two models. The differences in the model parameters used are listed in Table 1.

The model that was generated using Code I has a minimum cell size of 125 x 125 x 10 m. The layer thickness increases logarithmically with increasing depth of investigation until a maximum layer thickness of a 100 m is reached and stays constant thereafter. In addition to the topography, the bathymetry is also included in the model grid. The modelling was carried out over a frequency range from 0.0056 to 320Hz, using four frequencies per decade. The model grid has dimensions of 73 x 68 x 103 cells. Spurious data points were masked before running the inversion. A starting model with a homogeneous resistivity of 10 Ωm was used.

Table 1: Model parameters for the 3-D inversion of the data set using either Mackie's code (Code I) or Egbert's ModEM (Code II).

	Code I	**Code II**
Approach	Mackie (2012)	ModEM (Egbert & Kelbert, 2012)
Dimensions	73 x 68 x 103 cells	64 x 56 x 118 cells
Minimum cell size	125 x 125 x 10 meter	250 x 250 x 20 meter
Layer thickness	Increasing logarithmically; designed	Increasing logarithmically with 10%
Frequency range	0.0056 – 320Hz	0.001 – 250 Hz
Number of frequencies	20	28
Frequencies per decade	4	5
Initial model	10 Ωm	20 Ωm
Data inverted	Full tensor complex impedances	Off-diagonal complex impedances
Spurious data points masked	Yes	No
Topography	Yes	Yes
Bathymetry (Resistivity of sea water)	Yes (0.33 Ωm)	Yes (0.33 Ωm)
RMS	*1.53*	*2.3*
Number of iterations	*56*	*46*

When modelling with Code II, a grid with a minimum cell size of 250 x 250 x 20 m was used for the 3-D inversion. The layer thickness increases logarithmically at a constant rate of 10% within the depth of investigation, meaning that every layer is 10% thicker than the layer above it, until a layer thickness of 100 m is reached. Below a depth of about 3,000 m b.s.l. the layer thickness is again allowed to increase with a constant rate of 10%. With a grid size of 64 x 56 x 118 cells, a 300 x 300 km model grid is created with a maximum depth of 93 km. Both topography and bathymetry are included in the model grid design. The MT data were left un-rotated and the full tensor was modelled, without masking any spurious data points, in the frequency range from 0.001 to 250 Hz with five frequencies used per decade. An initial model with a constant resistivity of 20 Ωm was used.

It is obvious from Table 1 that the model produced using Code I will deliver a less "blocky" looking model since both the minimum cell size and the maximum layer thickness are considerably smaller than the model setup for Code II. The frequency ranges modelled are comparable, but more frequencies are modelled using Code II.

In addition to the two 3-D modelling codes used, the users of Code I also ran a 1-D inversion on the MT station responses. To this end they used the 1-D code developed by Rodi and Mackie (2001). The data were prepared similarly as described before and a 1-D model was derived for every station using the invariant of the impedance tensor. Running both a 1-D and a 3-D inversion on the same MT data set is a good consistency and data quality check.

The users of Code II also generated some 1-D inversion resistivity models to check the consistency of their 3-D results. This 1-D modelling was carried out using the same code as used by the users of Code I, as described above. The same data preparation as mentioned earlier was used.

4.1 Results - Code 1

The results derived from the 3-D inversion using Code I are presented as north-south and west-east running resistivity profiles and resistivity maps at constant elevation. In Figure 5, a profile running from north to south is presented. In this profile we see the typical structure of a very low resistivity layer overlying a high resistivity structure. Considering the local geology of the area, this low resistive structure might correspond with a conductive sedimentary basin sitting on top of a more resistive basement formation, possibly a limestone. It can also be observed in Figure 5 that the 1-D and the 3-D model results are in good agreement with each other.

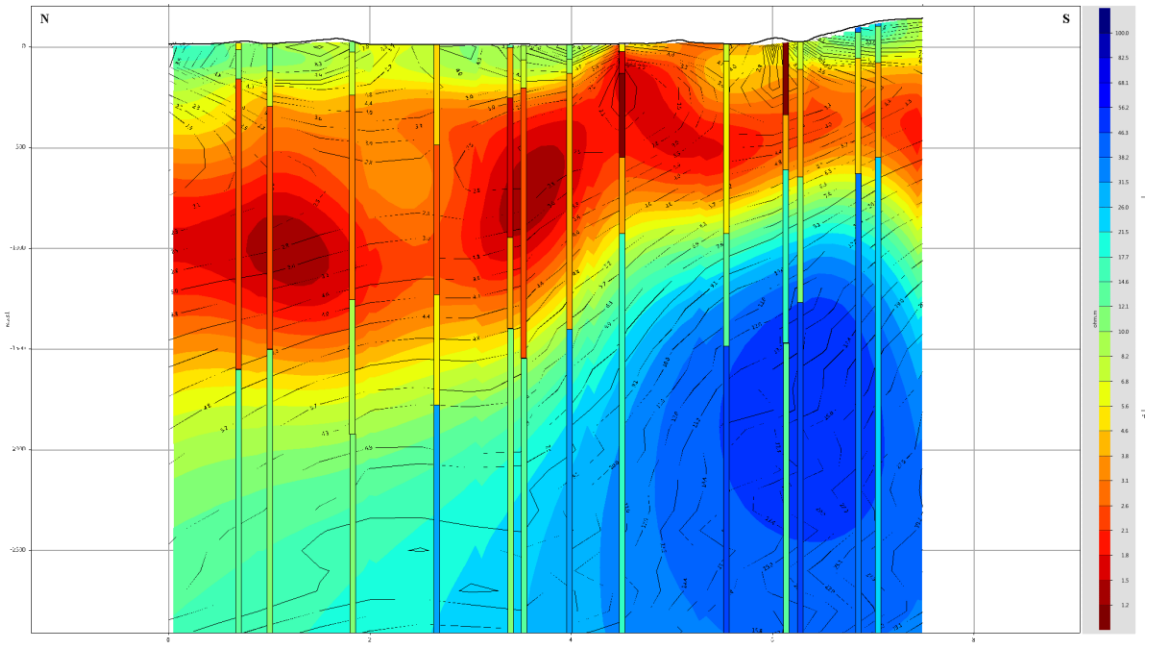

Figure 5: North-south oriented resistivity profile (profile NS_PA in Figure 2) of the 3-D inversion model results of Code I. At every measured MT station the layered 1-D inversion model is also plotted. The contour lines shown are an interpolation of the Occam 1-D inversion models at each site. All stations on this profile were measured using Metronix equipment.

When looking at the resistivity maps at constant elevation, a similar conclusion - a low resistivity overlying a high resistivity body - can be reached. Two of these maps at different depths are shown in Figure 6. Especially at the northeastern corner of the survey area, a low resistivity layer - possibly consisting of clay alteration minerals - is observed lying on top of a resistivity structure.

The low resistivity observed in the south of the survey area might be related to the presence of Pliocene sediments and Quaternary alluvium. Low resistivities near the seashore in the south are likely a combined effect of the conductive sea water and water saturated sediments.

4.2 Results - Code II

The 3-D inversion results of Code II are also presented as east-west and north-south oriented profiles, as well as resistivity maps at constant elevation. In Figure 7, approximately the same profile as presented in Figure 5 is plotted. Again, in this profile a low

resistivity layer is observed overlying a resistive structure. Several shallow low and high resistivity anomalies are observed as well. These are possibly related to static shift effects. These static shift effects in the resistivity model can be identified down to maximum depths of about 200 meter b.s.l.

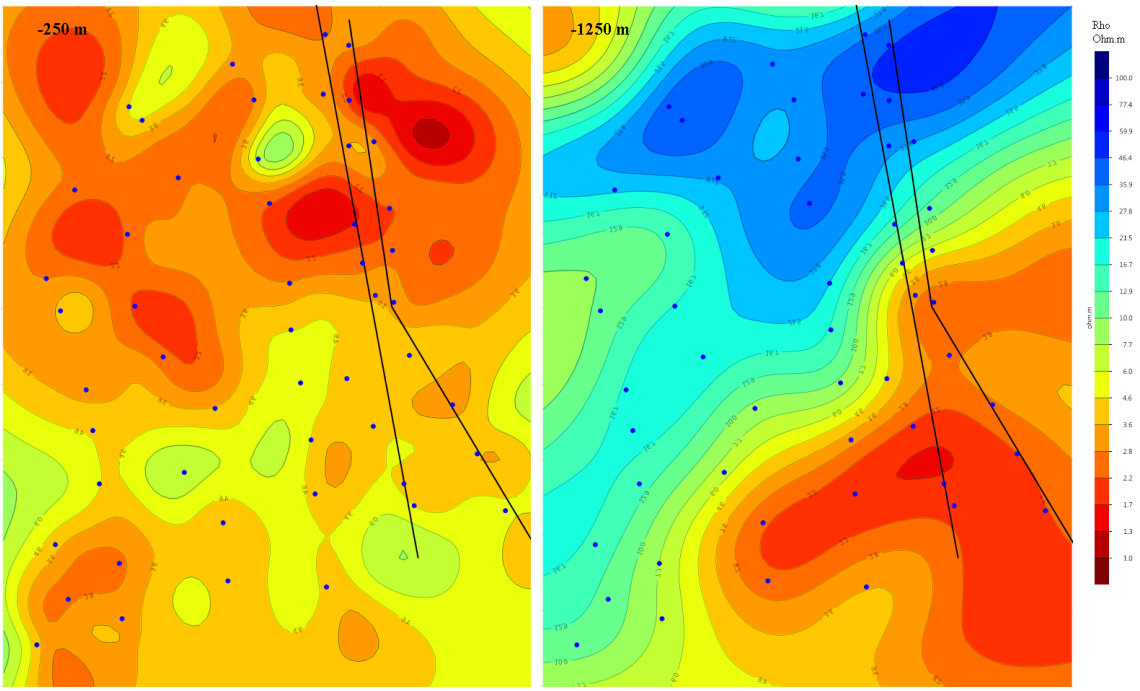

Figure 6: 250 meter b.s.l. elevation resistivity map of the survey area (left) and 1,250 meter b.s.l. elevation resistivity map of the 3-D inversion model (right) of Code I. Indicated on the map are the MT stations as well as the resistivity profiles.

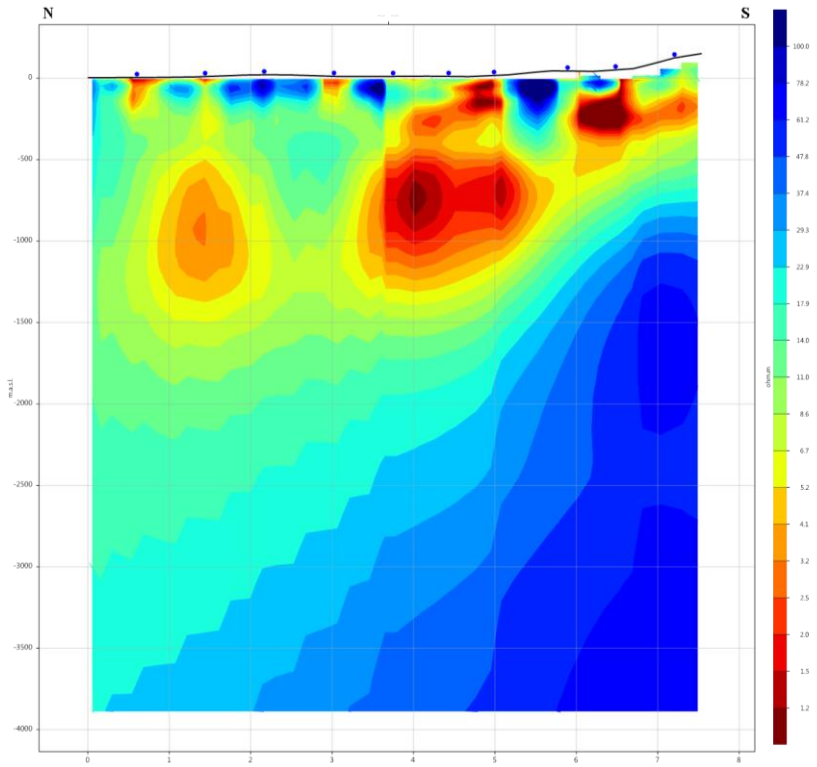

Figure 7: Roughly north-south oriented resistivity profile (Profile NS_PB in Figure 2) from the 3-D inversion model result of Code II. All stations in this profile were measured using Metronix equipment.

Resistivity maps at constant elevation, as shown in Figure 8, confirm the existence of a low resistivity layer above a structure with a higher resistivity.

The dissimilarities between the 1-D inversion and the 3-D inversion results are significant. This is especially clear in the southern part of the area as shown in Figure 9. Whereas in the 3-D model the low resistivity layer appears to be dipping towards the north,

the 1-D profile also plotted in Figure 9 gives the impression that this high conductivity layer is almost horizontal without any significant changes in depth or thickness towards the west. Again, in the 1-D result in Figure 9, some shallow anomalies are identified, in this case being less isolated than in the 3-D result and showing a better continuity within the resistivity profile. However, this apparent continuity might in fact be a misleading result and the shallow anomalies could also be the effect of either static shift or of the unmasked spurious MT data points.

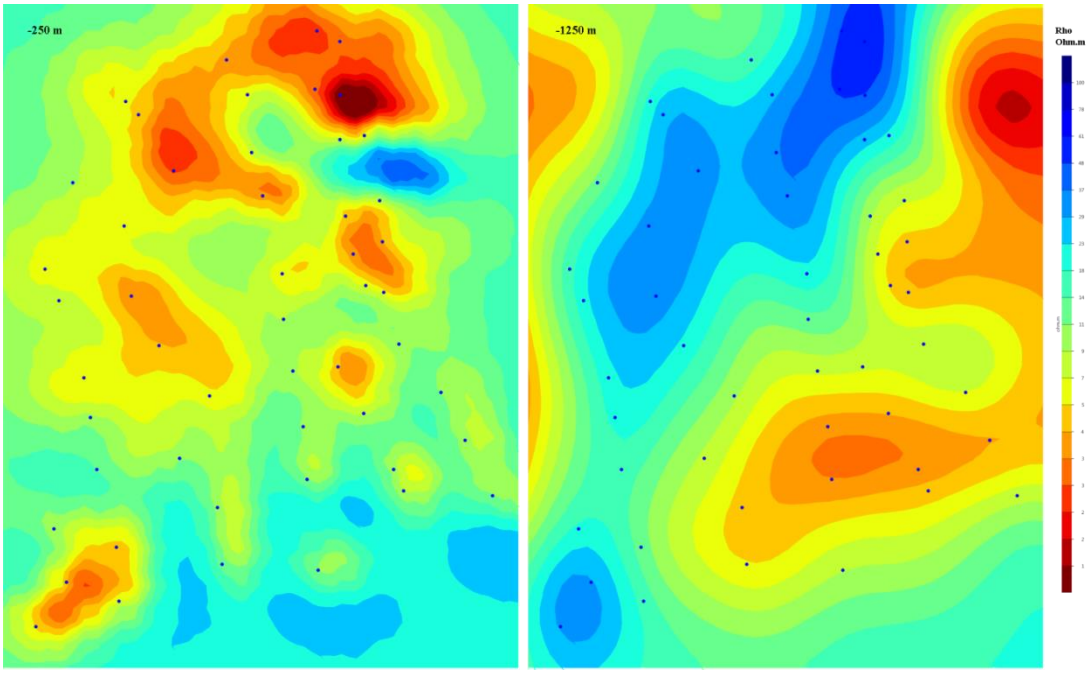

Figure 8: Result of the 3-D inversion modelling using Code II at 250 meter b.s.l. (left) and 1,250 meter b.s.l. (right). Station locations are indicated on both maps.

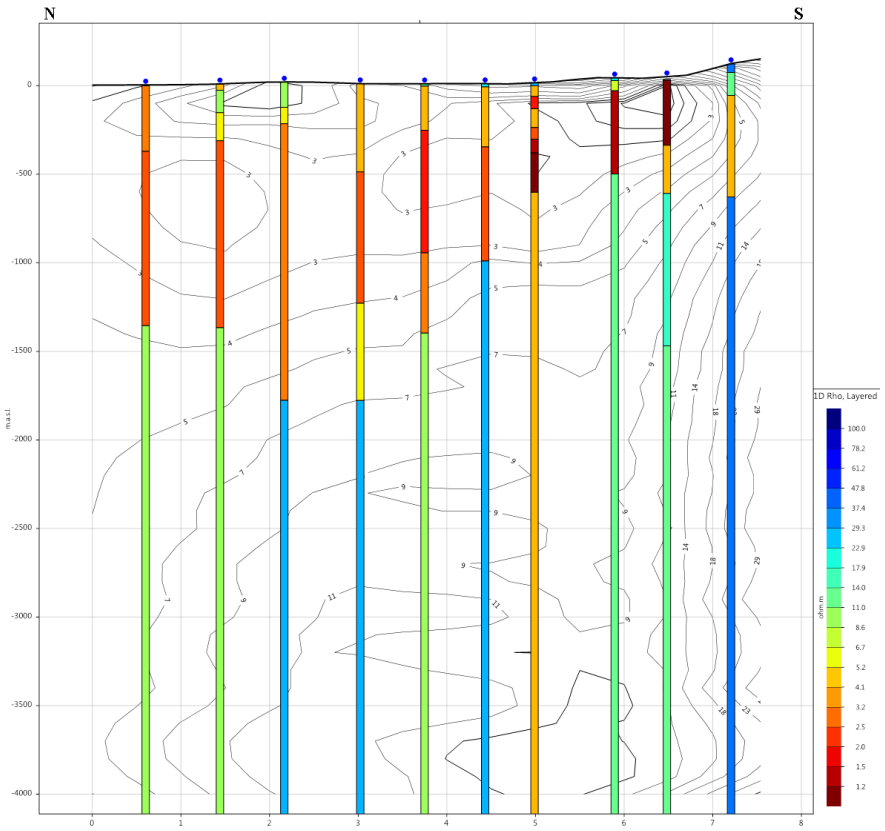

Figure 9: Interpolated 1-D inversion model for the same north-south oriented resistivity profile (profile NS_PB) as presented in Figure 7. At every measured MT station the layered 1-D inversion model is also plotted. The contour lines shown are an interpolation of the Occam 1-D inversion models at each site. All stations on this profile were measured using Metronix equipment.

4.3 3-D modelling results Code I and Code II compared

Although roughly showing the same large scale resistivity features, some significant differences between the 3-D modelling results from Code I and Code II can be identified.

First of all is there an obvious difference in the smoothness of the generated models when comparing Figure 5 and Figure 7, with the model generated with Code I (Figure 5) being the smoother (less "blocky") one. This is most likely a result of the smaller model cell size being used by Code I within the area of interest of the model grid. Another plausible explanation is the gridding algorithm used when plotting and presenting the data points on a profile or resistivity map. Apparently no gridding was performed when plotting the results of Code II, while a gridding algorithm was applied when plotting the results of Code I.

Secondly, there are near surface anomalies visible in the modelling results from Code II (Figure 7). These anomalies might best be explained by either static shift effects (e.g., Cumming, 2010; Árnason, 2010) or, which is more likely since no static shift corrections were made when using either Code I or Code II, by the fact that bad points in the input MT data are not masked before modelling in the case of Code II. It is very likely that the resistivity model for the prospect area can be improved significantly when thoroughly assessing and preparing the MT data before starting any 3-D inversion modelling.

Finally, while the resistivity values of the large anomalies seem to be consistent, there are some differences between the resistivity structures resolved by both codes. The main differences can be found at depths below approximately 1,000 meter b.s.l. where the low resistivity layer appears to fade at shallower depths in the results of Code II compared to the results of Code I. This can be observed in Figure 6 and in Figure 8. This may be the result of differences in the initial model or input data used by both groups. Whereas the users of Code II used the full tensor for their inversion, the users of Code I excluded the tipper data from the model input.

5. CONCLUSIONS AND FURTHER WORK

The MT data modelled and interpreted in this work is of average quality, but is difficult to assess since the data were acquired and processed in two parts, using different instruments and processing codes. It would probably be worthwhile to re-process all the data from the time series data, using a single processing routine.

The tipper data of the MT stations recorded with Phoenix instruments remain problematic for reasons yet not well defined.

Due to the different 3-D modelling strategies and parameters used, it is difficult to compare the results of the two different inversion codes. In general the 3-D results of the two codes are consistent with each other and with the results of comparative 1-D modelling, although there are some differences. While the large scale resistivity structures resolved by all models are expected to be present in the subsurface, this doesn't hold for the smaller resistivity anomalies. These small scale resistivity anomalies would however, be interesting to study in more detail when running a new 3-D inversion. This could be achieved by re-running Code II using the same modelling strategy as used when running Code I.

It is furthermore very reassuring that the absolute resistivity values show comparable values. The results of both models seem to confirm the geological structure of the survey area, with conductive sediments overlying a resistive base layer, probably limestone.

ACKNOWLEDGMENTS

The authors would like to thank Transmark Renewables Products B.V. for the opportunity to work with their resistivity data.

REFERENCES

Árnason, K., Eysteinsson, H., and Hersir G.P.: Joint 1D inversion of TEM and MT data and 3D inversion of MT data in the Hengill area, SW Iceland, *Geothermics*, **39**, (2010), 13-34

Cumming, W., and Mackie, R.: Resistivity Imaging of Geothermal Resources Using 1D, 2D and 3D MT Inversion and TDEM Static Shift Correction Illustrated by a Glass Mountain Case History, *Proceeding*, World Geothermal Congress 2010, Bali, Indonesia, (2010).

Egbert, G.D., and Booker, J.R.: Robust Estimation of Geomagnetic Transfer Functions, *Geophysics Journal of the Royal Astronomical Society*, **87**, (1986), 173-194.

Egbert, G.D., and Kelbert, A.: Computational Recipes for Electromagnetic Inverse Problems, *Geophysical Journal International*, **189**, (2012), 251-267.

Jones, A.G., Chave, A.D; Egbert, G., Auld, D., and Bahr, K.: A Comparison of Techniques for Magnetotelluric Response Function Estimation, *Journal of Geophysical Research*, **94**, (1989), 14,201-14,213.

Mackie, R., and Watts, M.D.: Detectability of 3-D sulphide targets with AFMAG, *SEG Technical Program Expanded Abstracts*, (2012), 1-4.

Parker, R.L, and Whaler, K.A.: Numerical Methods for Establishing Solutions to the Inverse Problem of Electromagnetic Induction, *Journal of Geophysical Research*, **86**, (1981), 9574-9584.

Parker, R.L. and Booker, J.R.: Optimal one-dimensional inversion and bounding of magnetotelluric apparent resistivity and phase measurements, *Physics of the Earth and Planetary Interiors*, **98**, (1996), 269-282.

Rodi W., and Mackie R.L.: Nonlinear conjugate gradients algorithm for 2-D magnetotelluric inversion, *Geophysics*, **66**, (2001), 174-187.M001

Şerpen, U., Aksoy, N., Öngür T., and Didem Korkmaz, E.: Geothermal energy in Turkey: 2008 update, *Geothermics*, **38**, (2009), 227-237.